NOTES AND CORRESPONDENCE

On the Potential Impact of Daytime Surface Sensible Heat Flux on the Dissipation of Martian Cold Air Outbreaks

M. SEGAL AND R. W. ARRITT

Agricultural Meteorology, Department of Agronomy, Iowa State University, Ames, Iowa

J. E. TILLMAN

Department of Atmospheric Sciences, University of Washington, Seattle, Washington

16 April 1996 and 15 November 1996

ABSTRACT

The Martian daytime soil surface temperature is governed primarily by the net irradiance balance and surface soil heat flux. Thus the outbreak of a cold air mass generates increased sensible heat flux that is conducive to daytime dissipation of the cold air mass thermal characteristics. Conceptual and scaling evaluations of this dissipation are provided while comparison is made with similar situations on Earth. It is estimated that sensible heat flux contribution to the dissipation of the original thermal structure of the cold air could be three times larger than the corresponding situation on Earth. Illustrative numerical model simulations provide scaling of the potential impact on the dissipation of cold air masses for various combinations of background wind speed and latitudes.

1. Introduction

The daytime Martian surface thermal energy balance is predominantly governed by net irradiance fluxes and surface soil heat flux (e.g., Kieffer et al. 1977). Because of the low density of the Martian atmosphere (see Table 1 for typical values of surface atmospheric pressure), the surface sensible heat flux H_s is secondary in its effect on the surface energy balance but is a prime thermal source in the onset of daytime convective boundary layer (CBL) characteristics. Typical daily averaged values of incoming solar irradiance on a horizontal surface in the midlatitudes during the northern hemisphere spring equinox ($L_s = 0°$; where L_s is areocentric longitude of the sun) accounting for dust opacity effects are ~200–300 W m^{-2}, whereas in winter ($L_s = 270°$) the values are 75–175 W m^{-2} (Applebaum et al. 1993). The daytime averaged incoming longwave irradiance at the surface emitted by the Martian atmosphere for winter–early spring atmospheric temperatures is <30 W m^{-2} for atmospheric dust optical depth τ less than 1 (inferred from Haberle and Jakosky 1991). Projections from Sutton et al. (1978) and Tillman et al. (1994) for the related values of the sensible heat fluxes H_s in midlatitude during winter and early spring periods of the Martian year are <20 W m^{-2} (the H_s values are sensitive to soil thermal inertia, surface roughness, and wind speed).

Therefore, during daytime outbreaks of cold air masses over relatively warm surfaces, only a mild effect of sensible heat transfer on the soil surface temperature is anticipated. The commencement of a cold air outbreak should result in an increased atmosphere–surface potential temperature difference, $\Delta\theta$, and consequently an increase in H_s. Enhanced wind speeds may be associated with these events, further increasing the values of H_s (Tillman et al. 1994). The increased H_s values should be conducive to dissipation of the cold air mass thermal characteristics. Evaluations of the effects of surface sensible heat flux on cold air outbreaks have not been reported, and it is the objective of this note to provide an initial estimation of these characteristics.

Some of the above surface effects on H_s values on Earth's frontal systems are evaluated by Sanders (1955). On Earth, the soil surface temperature adjusts rapidly to air temperature change following passage of a cold air mass (e.g., Mahrer and Segal 1984). The Martian scenario, however, is to some extent analogous to outbreaks of continental cold air over Earth's relatively warm oceans. The heat storage of the oceanic surface layer is almost unaffected by the outbreak; thus the water surface temperature is only mildly modified in most cases. Consequently, the enhanced H_s values during

Corresponding author address: Moti Segal, Agricultural Meteorology, Department of Agronomy, Iowa State University, Ames, IA 50011.

TABLE 1. Input parameters for the numerical simulation.

Model top	28 km
Number of atmospheric levels	41 (the lowest 10 levels are 1.6, 10, 25, 50, 100, 175, 300, 500, 750, and 1000 m)
Background wind speed	3, 6, 9, 12, 15, 18, 21, 24, 27 m s^{-1}
Areocentric longitude of the sun (L_s)	0° (vernal equinox)
Surface pressure based on VL-1 and VL-2 sites	VL-1: 8.2 mb; VL-2: 8.8 mb
Atmospheric dust optical depth	0.6
Surface roughness parameter	1 cm
Solar constant	563 W m^{-2}
Solar declination angle	0°
Surface albedo	0.3
Number of soil module levels	20
Soil thermal inertia	260 W m^{-2} $s^{½}$ K^{-1}

such events result in significant modification of the cold air mass thermal characteristics within a relatively short period (e.g., Garratt 1992). Projecting from the Earth marine case, it is likely that analogous rapid modifications are caused by the daytime cold air outbreaks on Mars.

Tillman et al. (1979) survey earlier studies evaluating existence of northern hemisphere Martian frontal systems. They were first to infer the passage of cold fronts, based on Viking L-2 measurements. Horizontal temperature differences as high as 20 K were inferred across the cold front at Viking Lander site L-2 (48°N). Infrared interferometer spectrometer analysis by Santee and Crisp (1993) implies that differences in the lower atmosphere temperature of 30 K across a narrow zone of the CO_2 polar ice cap edge are likely during the late northern winter. (The Martian atmosphere consists of about 95% CO_2. Condensation and sublimation of CO_2 produces annual variation of the ice cap size.) Generally, outbreaks of intense cold air masses are attributed to baroclinic wave activity associated occasionally with advection to the midlatitudes of cold polar air masses. It is suggested that considerable dissipation of any cold front or outbreak of cold air mass can occur within short timescales, due to the increase in daytime H_s values resulting from the abrupt drop in the atmospheric temperature.

In the evaluations presented in this note a Lagrangian approach is adopted, in which an atmospheric column is followed in time along a given latitude, and the impact of the surface sensible heat flux on its thermal structure is evaluated. A bulk scaling of such effects as well as conceptual evaluations are provided in section 2. The impacts of surface sensible heat flux on the thermal structure of cold fronts on Earth have been found to be important in various situations (e.g., Segal et al. 1993a; Miller et a1. 1996). Therefore, comparisons of similar situations of cold air outbreaks on Mars and Earth are useful and were included in the scaling. The effect of variation in wind speed, consideration of longwave irradiance flux divergence, as well as the time dependence of the atmosphere–soil thermal interaction, are not included in the bulk scaling. Therefore, numerical modeling of the thermal interactions during Martian cold air outbreaks would provide complementary scaling. Evaluations of the impact of wind speed, $\Delta\theta$, and the solar irradiance (as dependent on latitude) on the boundary layer thermal characteristics for an illustrative case of cold air outbreaks are made by utilizing a 1D numerical boundary layer model, as described in section 3. The model evaluation consists of comparisons of simulated thermal characteristics of control runs against those simulated in prescribed cold air outbreak runs.

2. Conceptual evaluations

In the analysis of atmospheric thermal modifications by the sensible heat flux, a Lagrangian column of a cold air mass is followed along a given latitude and its boundary layer thermal modifications are scaled. Thus the potential dissipation of cold air mass thermal characteristics can be projected. Since the magnitude of H_s at night is about one order of magnitude lower than the daytime value (with opposing sign), only the daytime period is considered in the present evaluations. For scaling purposes, it is assumed that in the morning (around sunrise) the lower atmosphere has an average vertical potential temperature gradient, β_0. The daytime average potential temperature increase within the CBL, due to the sensible heat flux contribution at time, t, later in the day is denoted θ' and it can be approximated as

$$\bar{\theta}' = \frac{1}{2}\bar{\beta}_0 h_t, \tag{1}$$

where h_t is the depth of the CBL at time t. The value of θ' acquires its peak near the surface and in a first approximation drops linearly to 0 at height h_t. A common approximation of the value of h_t at time t following sunrise (e.g., Garratt 1992) is

$$h_t = \left[\frac{2C_\theta \int_0^t H_s\, dt'}{\rho C_p \bar{\beta}_0}\right]^{1/2}, \tag{2}$$

where C_θ ($\approx$1.2) is an entrainment coefficient considering the downward heat flux at the CBL top, C_p is the

atmospheric heat capacity at constant pressure, and ρ is the average density within the CBL. In order to facilitate general insight into the characteristics of modification of cold air masses on Mars, comparison is made with Earth. Denoting by subscript m and e, Martian and Earth parameters, respectively, and substituting the corresponding values of ρ and C_p on Earth and Mars into (1) and (2), it follows that

$$\eta = \frac{\bar{\theta}'_{\mathrm{m}}}{\bar{\theta}'_{\mathrm{e}}} \cong 8\left[\frac{\bar{\beta}_{\mathrm{om}}}{\bar{\beta}_{\mathrm{oe}}}\right]^{1/2}\left[\frac{\hat{H}_{\mathrm{sm}}}{\hat{H}_{\mathrm{se}}}\right]^{1/2}, \tag{3}$$

where $\hat{H}_s$ is the integrated sensible heat flux by time t. Adopting, in a conservative approach, $[\hat{H}_{\mathrm{sm}}/\hat{H}_{\mathrm{se}}]^{1/2} \leq 0.26$ (assuming at noon $H_{\mathrm{sm}} \leq 20$ W m^{-2} and $H_{\mathrm{se}} \leq 300$ W m^{-2}; note that during cold air outbreaks on Earth the surface latent heat flux is suppressed) and $\bar{\beta}_{\mathrm{om}} = 2\bar{\beta}_{\mathrm{oe}}$ results in $\eta \leq 3$. Thus the effect of daytime surface sensible heat flux on the dissipation of the cold air outbreak during winter–early spring may be in a first approximation as much as about three times larger on Mars than on Earth [Ye et al. (1990), estimated for the summer $\eta \cong 3.5$].

The surface sensible heat flux is provided by the relation

$$H_S = -\rho_Z C_p C_H u_Z(\theta_Z - \theta_s), \tag{4}$$

where C_H is the near-surface heat transfer coefficient (sensitive to surface layer Monin–Obukhov length), u_Z, θ_Z, ρ_Z, and θ_s are the near-surface (at height Z) wind speed, potential temperature, air density, and the ground surface potential temperature, respectively.

The interrelationship between u_Z and $(\theta_Z - \theta_s)$ in Eq.(4) in controlling H_s on Earth and Mars is evaluated in the following. During the daytime on Earth over land, intensification of u_Z results in an immediate response of some increase, ΔH_s, in the sensible heat flux (typically for common range of daytime wind speed $[\Delta H_s] \sim 0.1$ $[H_s]$). Such increases in H_s are sufficient to reduce noticeably the surface potential temperature θ_s. On Mars, where θ_s is primarily forced by the net radiative balance, the absolute ΔH_s value due to the change in u_Z is smaller than on Earth and the corresponding perturbation of θ_s is mild. Thus, H_s values on Mars would *relatively* increase more than on Earth with initiation of enhanced u_Z. However, gradual decrease with time in H_s values would result due to the increase in θ_Z.

From Eqs. (1)–(2), θ' and h are proportional to $\hat{H}_s^{1/2}$. Thus the increase of H_s with u_z would result in stronger dissipation of the cold air mass through a deeper vertical extent. Note that, for scaling purposes, in Eq. (2) the average value of β_0 within the CBL depth h_t was considered. Since β_0 decreases with height, deeper CBL would reduce $\bar{\beta}_0$, which, from (2), is conducive for further CBL growth. For example, when H_s is doubled, h would increase by a factor greater than $\sqrt{2}$ because of the reduction in β_0 with height.

Finally, commencement of an equatorward Martian cold air mass outbreak around sunset, in a given geographical location, would likely distort only mildly the downwind air mass thermal stratification during the nocturnal period due to suppression of the $|H_s|$ values (most of the effect is likely near the surface). Therefore, in such situations the equatorward expansion of the cold air outbreak effectively increases. For example, a northerly wind component of 20 m s^{-1} causes equatorward advection during the night (~12 h) to be ~890 km, which is about 15° latitude.

3. Numerical modeling

a. Modeling aspects

An illustrative case reflecting late winter–early spring ($L_s = 0°$) conditions was simulated. The Earth numerical mesoscale model, whose formulation is given in detail in Arritt (1989), was converted to a Martian model. The model uses a turbulence closure in which the turbulent fluxes are derived with the aid of prognostic turbulent kinetic energy equation and diagnostic length scale. The soil module consists of a heat conduction equation solved in multilevel grid points (with increased resolution near surface). At the surface the thermal fluxes are accounted for in the determination of the top layer soil temperature. This model adjustment to the Martian atmosphere was accomplished by adjustments of physical constants and by implementing the Martian radiative transfer scheme following Savijarvi (1991). Included are solar irradiance transfer considering atmospheric CO_2 and dust effects, and CO_2 infrared transfer using an emissivity scheme. Dust effects in the infrared are not considered (however, this should have only a secondary effect on the dissipation of the cold air outbreak since for the dust optical depth values considered, the corresponding daytime effect on the surface temperature is small).

The computational procedure outlined in Segal et al. (1993b) was used for carrying out illustrative multiple 1D model simulations. (The procedure utilizes a 3D numerical model array in which all formulations for atmospheric horizontal processes are removed, and the horizontal spatial coordinates are replaced by parameter ranges.) Pertinent combinations of geostrophic wind speed, U_g, (ranging from 3 to 27 m s^{-1}) and latitude (ranging from 35°N to 55°N) were considered. Note that the predicted near-surface wind speed is lower than U_g due to frictional effects. The model basic input parameters used in the simulations are provided in Table 1.

A steady radiative–convective equilibrium for the diurnal cycle was established following 120 h of simulation. From this stage (0600 Martian sun time or MST), which reflects the initial conditions, the simulations were continued for an additional 33 h, considering two situations: (i) control simulation, which consisted of an extension of the original simulation through its equilibrium stage, and (ii) cold air outbreak in which a pre-

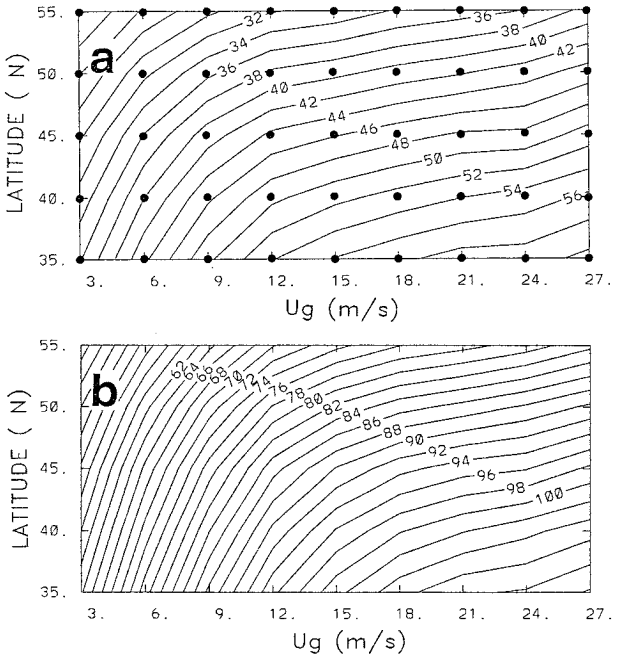

FIG. 1. Accumulated sensible heat flux, $\hat{H}_s$, (10^4 W m^{-2}) following 33 h of simulation for (a) the control simulation (the dark circles indicate the various 1D simulations in the composite and their corresponding background flow values, U_g, and latitude), and (b) cold air outbreak simulation.

scribed drop in the potential temperature constituted an analogous situation to the initiation of passage of cold front and subsequent advection of cold air mass. The potential temperature composites in both situations following 33 h of simulation (i.e., at 1500 MST of the next day) are presented. The atmospheric dust optical depth values adopted in the simulated days are those measured at VL-1 and VL-2 [Colburn et al. (1989), Fig. 1; the lowest values were adopted]. In the presented results, the unperturbed simulations reflect the warm air mass sector, whereas the perturbed simulation reflects the cold air mass sector. Comparing both provides insight into the potential changes in horizontal thermal gradients while ignoring the supply of cold air by advection (see evaluations in Segal et al. 1993a). Finally, it is worth noting that the maximum drop in the noon soil surface temperature in the cold air outbreak simulation compared with the control simulation was ~4 K (for strong U_g) and reduced gradually to ~0 K with the decrease in U_g (not shown). This is in agreement with the evaluation in the previous section.

b. Simulation results

Figure 1a presents a composite in the parameter space U_g–Latitude of the accumulated sensible heat flux $\hat{H}_s$ contributed into the atmosphere following 33 h of the control simulation. The composite consists of 45 1D simulations representing the various combinations for the indicated U_g and latitude values (each 1D simulation of the composite is represented by a dark circle in Fig. 1a). Reduction of $\hat{H}_s$ while moving northward results from the decrease in solar irradiance. The rate of increase of $\hat{H}_s$ with the wind speed U_g is most pronounced for the lower range of U_g values. For the high range of U_g values, the variations in $\hat{H}_s$ are much less pronounced as the near-surface air temperature is higher in response to the increased values of $\hat{H}_s$ (see discussion in section 2). In the cold air outbreak simulation (Fig. 1b), where the lower 4.5 km of the atmosphere was initially (0600 MST) cooled by 25 K (e.g., reflecting cold air outbreak originating over the CO_2 ice cap), a sharp increase in $\hat{H}_s$ resulted in response to the increase in $|\theta_z - \theta_s|$. The values of $\hat{H}_s$ are about doubled when compared with those in the control simulation. The contribution to $\hat{H}_s$ was most pronounced immediately following the imposition of the temperature drop and gradually declined with the progress of the simulation (not shown). The magnitude of the increase in $\hat{H}_s$ implies, based on the previous scaling, substantial warming of the lower atmosphere compared with the control simulation.

Figure 2a presents the composite in the parameter space Z–U_g for the potential temperature θ at latitude 45°N at the commencement of the control simulation (0600 MST). Intense radiative surface inversions within a depth of several hundred meters above ground were simulated. At 1500 MST the next day, following 33 h of simulation (Fig. 2b), the CBL depth ranged from ~1.3 km to ~2 km for the given range of wind variation (the CBL is taken as the depth of the lower atmosphere layer in which $\partial\theta/\partial z \leq 0$). In the cold air outbreak simulation following 33 h (Fig. 2c), the CBL is noticeably deeper compared with the control simulation. The depth of the CBL about doubled compared with that of the control simulation. Comparing Figs. 2b and 2c shows that for $U_g = 27$ m s^{-1}, for which the highest $\hat{H}_s$ were simulated, θ values in the cold air outbreak simulation were lower only by ~6 K near the surface and by ~7 K at the height corresponding to the top of the CBL in the control simulation (compared with 25 K in the commencement of the simulation). Differences in the longwave flux divergence between both simulations also affected the CBL warming feature. As discussed previously, the $\hat{H}_s$ impact reduces with wind speed; for U_g=3 m s^{-1} the potential temperature difference was ~9 K near the surface and at the top of the CBL (~1.3 km).

An illustrative latitudinal composite (Z–Latitude) depicting the impact on cold air mass dissipation for $U_g = 12$ m s^{-1} is presented in Fig. 3. Figure 3a shows the initial θ composite for the control simulation, and Fig. 3b shows the related composite following 33 h of simulation (1500 MST). The latitudinal variation of the CBL depth (and its potential temperature) is noticeable. Figure 3c depicts the related composite following 33 h of the cold air outbreak (where in the lower 4.5 km the initial θ were 25 K lower than in the control simulation).

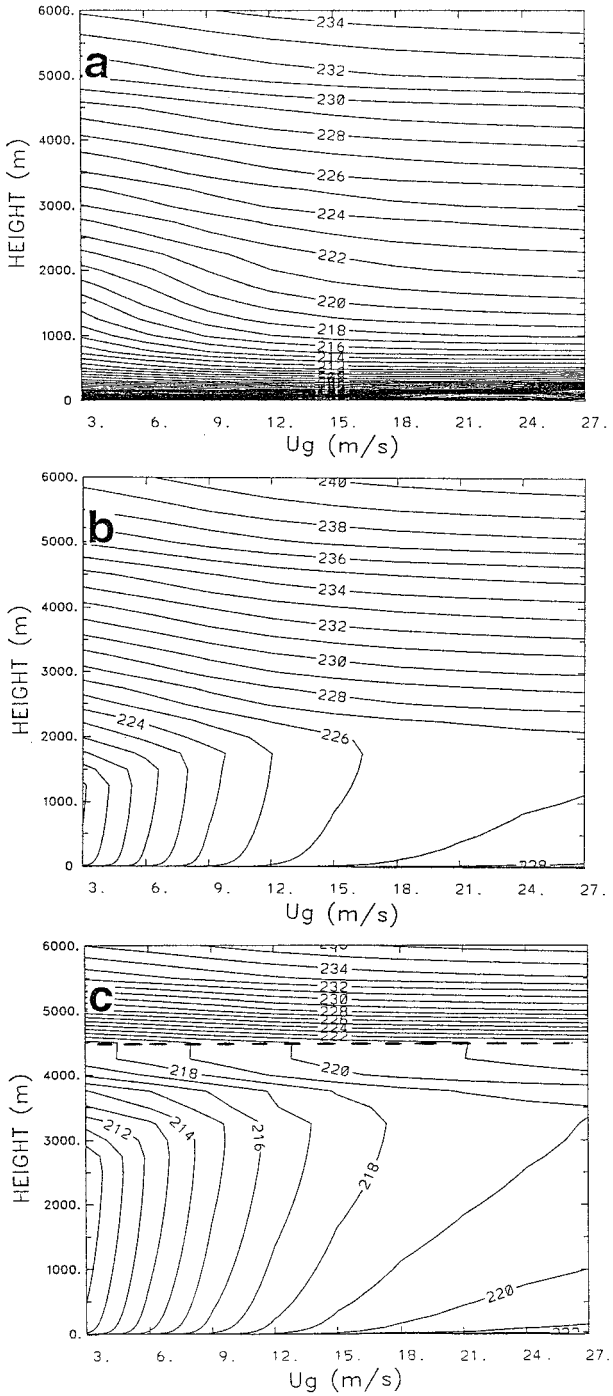

FIG. 2. Z–U_g composite of the potential temperature θ (K) at latitude 45°N (a) at the commencement of the control simulation (0600 MST), (b) following 33 h of the control simulation (1500 MST), and (c) as (b) except for the cold air outbreak simulation (in the layer confined by the dashed line, initially the potential temperature values were reduced by 25K).

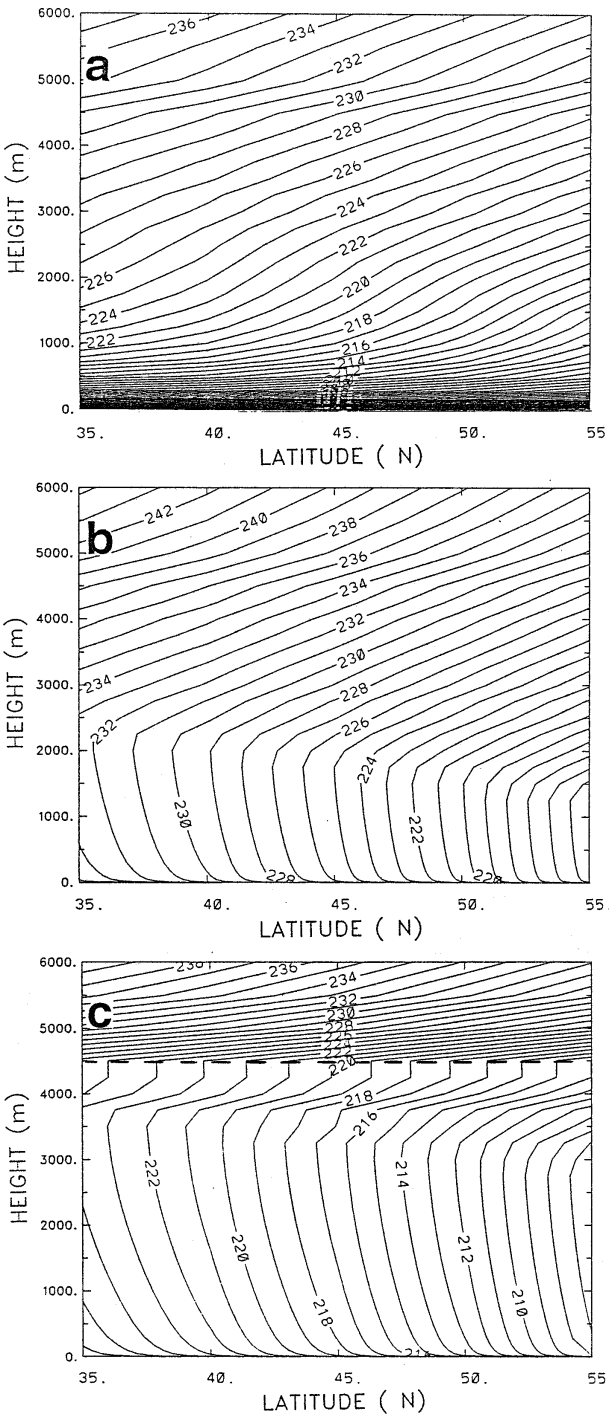

FIG. 3. Z–Latitude composite of the potential temperature θ (K) for $U_g = 12$ m s^{-1} (a) at the commencement of the control simulation (0600 MST), (b) following 33 h of the control simulation (1500 MST), and (c) as (b) except for the cold air outbreak simulation.

The deepening of the CBL and the eroding of the cold air are significant, especially at high latitudes. Near-surface θ values were lower only by ~8 K at latitude 35°N and by ~7 K at latitude 55°N compared with the corresponding values in the control run (i.e., the near-surface warming magnitudes were 17 K and 18 K, respectively).

Finally, observations of maximum daily air temper-

ature and mean wind speed at 1.6 m in the two Viking Lander sites, VL-1 (22°N) and VL-2 (48°N), are presented in Tillman et al. (1994). For $L_s = 0°$, the maximum temperature is available only at VL-2, where a value of ~217 K is representative (the daytime observed characteristic wind speed corresponds to $U_g = 12$ m s^{-1}). The 1500 MST simulated 1.6-m temperature (which is also about the maximum temperature) at 48°N is ~223 K (Fig. 3b), in reasonable agreement with the observed temperature.

4. Conclusions

Scaling and illustrative numerical model simulations presented in this note quantify the potential effect that the daytime surface sensible heat flux has on the suppression of equatorward outbreak of Martian cold air masses. Scaling indicates that this process may be as much as three times more effective in modifying the cold air mass compared with equivalent situations on Earth. Simulations were carried out reflecting northern hemisphere late winter–early spring solar conditions. Adopting a Lagrangian approach and tracing an atmospheric column of cold air advected along a given latitude, it was found in the model simulations that the original thermal characteristics of the atmosphere are considerably modified due to warming following 33 h. Faster decrease in frontal thermal contrast or in thermal characteristics of cold air outbreak should occur with equatorward movement of a cold air mass, as a result of the increase in solar irradiance and the sensible heat flux.

Acknowledgments. The research was supported by NASA Grant, NAGW-4060 and NAGW-3381. We would like to thank N. Johnson for help with the Viking data and C. Daniel for his assistance. R. Diedrichs prepared the manuscript.

REFERENCES

Applebaum, J., G. A. Landis, and I. Sherman, 1993: Solar radiation on Mars—Update 1991. *Sol. Energy,* **50** (1), 35–51.

Arritt, R. W., 1989: Numerical modeling of the offshore extent of sea breezes. *Quart. J. Roy. Meteor. Soc.,* **115,** 547–570.

Colburn, D. S., J. B. Pollack, and R. M. Haberle, 1989: Diurnal variation in optical depth at Mars. *Icarus,* **79,** 159–189.

Garratt, J. R., 1992: *The Atmospheric Boundary Layer*. Cambridge University Press, 316 pp.

Haberle, R. M., and B. Jakosky, 1991: Atmospheric effects on the remote determination of thermal inertia on Mars. *Icarus,* **90,** 187–204.

Kieffer, H. H., T. Z. Martin, A. R. Peterfreund, E. D. Miner, and F. D. Palluconi, 1977: Thermal and albedo mapping of Mars during the Viking primary mission. *J. Geophys. Res.,* **82,** 4249–4291.

Mahrer, Y., and M. Segal, 1984: Model evaluation of the impact of perturbed weather conditions on soil-related characteristics. *Soil Sci.,* **140,** 368–375.

Miller, L. J., M. A. LeMone, W. Blumen, R. L. Grossman, N. Gamage, and R. Zamora, 1996: The low-level structure and evolution of a dry arctic front over the central United States. Part I: Mesoscale observations. *Mon. Wea. Rev.,* **124,** 1648–1675.

Sanders, F., 1955: An investigation of the structure and dynamics of an intense surface frontal zone. *J. Meteor.,* **12,** 542–552.

Santee, M., and D. Crisp, 1993: Thermal structure and dust loading of the Martian atmosphere during late southern summer: Mariner 9 revisited. *J. Geophys. Res.,* **98,** 3261–3279.

Savijarvi, H., 1991: A model study of the PBL structure on Mars and Earth. *Beitr. Phys. Atmos.,* **64,** 219–229.

Segal, M., W. L. Physick, J. E. Heim, and R. W. Arritt, 1993a: The enhancement of cold front temperature contrast by differential cloud cover. *Mon. Wea. Rev.,* **121,** 867–873.

——, R. W. Arritt, and J. E. Heim, 1993b: A simple and efficient scheme for performing one and two-dimensional numerical model sensitivity experiments. *Mon. Wea. Rev.,* **121,** 1871–1873.

Sutton, J. L., C. B. Leovy, and J. Tillman, 1978: Diurnal variations at the Martian surface layer meteorological parameters during the first 45 sols at two Viking Landers sites. *J. Atmos. Sci.,* **35,** 2346–2355.

Tillman, J. E., R. M. Henry, and S. Hess, 1979: Frontal systems during passage of the Martian north polar hood over the Viking Lander 2 site prior to the first 1977 dust storm. *J. Geophys. Res.,* **84,** 2947–2955.

——, L. Landberg, and S. E. Larsen, 1994: The boundary layer of Mars: Fluxes, stability, turbulent spectra, and growth of the mixed layer. *J. Atmos. Sci.,* **51,** 1709–1727.

Ye, Z. J., M. Segal, and R. A. Pielke, 1990: A comparative study of daytime thermally induced upslope flow on Mars and Earth. *J. Atmos. Sci.,* **47,** 612–629.